Desalination and Water Treatment
www.deswater.com
doi: 10.5004/dwt.2023.29518

292 (2023) 69–83
April

Modeling of stormwater infiltration basin enhanced with drywells technique

Zakaria Helles[a,*], Yunes Mogheir[b]

[a]*Water Technology Ph.D. Joint Program, Islamic University of Gaza, and Al-Azhar University of Gaza, Palestinian Authority, Tel.: +970-599-860-432; email: zakaria.helles@gmail.com*
[b]*Civil and Environmental Eng., Islamic University of Gaza, Palestinian Authority, Tel.: +970-599-446-112; email: ymogheir@iugaza.edu.ps*

Received 19 February 2023; Accepted 3 April 2023

ABSTRACT

Harvesting of stormwater in the Gaza Strip is very important for the aquifer recharge since the stormwater infiltration is considered the sole replenishing source which reimburses the severe groundwater abstraction and protects the aquifer from unrecoverable deterioration. Gaza Strip experienced stormwater infiltration basins several years ago using different infiltration techniques. Waqf Basin is an existing stormwater infiltration basin located in Gaza City that used a surface natural infiltration technique, however, recently the basin was upgraded and augmented by drilling 18 boreholes (drywells) at zone 4 (western part of the basin). As a result, the basin has an improved infiltration capacity as revealed during the 2021–2022 wet season through field observation readings of water levels with a borehole infiltration capacity estimated as 111.0, 250, 316.7 m^3/d at 1.70, 3.40, 5.10 m ponded water depth, respectively. In addition, HYDRUS (2D/3D) software was used in this research to model/simulate Waqf Basin at ponded water depths 1.70, 3.40, and 5.10 m with the corresponding obtained borehole infiltration capacities as 289.0, 324.19, 250.39 m^3/d, respectively. The results emphasized that the single borehole infiltration capacity was in agreement with the field observed readings as the borehole infiltration capacity increases with the increase of basin ponded water depth. Nevertheless, the difference between HYDRUS and field observed results was attributed to the clogging effect which needs further studies in the future. Using the borehole infiltration technique is efficient when properly designed, implemented, and repaired at the end of each wet season to protect the system from permanent malfunctioning.

Keywords: Stormwater; Infiltration basin; Drywell; Ponded water depth; HYDRUS; Transport domain

1. Introduction

The Gaza Strip has long suffered from water scarcity, which is considered a worsening problem due to several factors that may lead to the permanent deterioration of groundwater resources. Stormwater recharge is the only low-cost and readily available method of replenishing Gaza Strip groundwater with fresh and clean water, which can alleviate and replenish the groundwater from excessive declination and thus seawater intrusion. More than 26 stormwater structures are currently in use in the Gaza Strip; 16 of them are categorized as stormwater infiltration basins using various infiltration techniques, and the remaining 10 are stormwater retention structures that serve as temporary detention basins [1].

They are all distributed over different Gaza governorates to capture the rainfall surface runoff during wet seasons and hence infiltrate the stormwater collected into the aquifer. In the past, the study of the unsaturated zone, referred to as the vadose or variably saturated zone, was for agricultural productive purposes; however, modeling of water flux and solute particles transport in this zone has increased

* Corresponding author.

1944-3994/1944-3986 © 2023 Desalination Publications. All rights reserved.

and progressed significantly during the recent decades, and a wide spread of utilization of newly developed applications was dominantly observed for predicting the water flow behavior as well as the movement of other solute components [2].

Infiltration basin modeling and simulation using a variety of computer programs is now possible owing to the advancements in numerical solutions. In this study, one of the local existent stormwater infiltration basins in Gaza city was modeled and simulated using one of the most well-known computer programs, HYDRUS (2D/3D).

Waqf Basin is a stormwater infiltration basin located in Gaza city which was studied extensively through field investigation to evaluate and assess the basin infiltration efficiency during the 2021–2022 wet season [3]. Then, the obtained results were compared to that obtained by the numerical solution as carried out in this research. The applied approach of stormwater infiltration at Waqf Basin was set as a second phase of repair and development of the basin, which comprised the stormwater infiltration through 18 drilled boreholes (boreholes and drywells are interchangeably used in this research) of 0.355 m diameter extending to a depth of 16 m underneath the basin floor surface as discussed by the study of Helles and Mogheir [4].

The surface infiltration through the basin floor was ignored, and the only infiltration of stormwater occurred through the drilled boreholes, which were non-backfilled but cased with UPVC pipes. The infiltration technique used in Waqf Basin is referred to as the vadose zone infiltration technique in which drywells infiltrate captured stormwater into the underneath soil profile, however, this research studied and evaluated the performance of the borehole infiltration capacity during the simulation time set by the software.

2. Methodology

HYDRUS (2D/3D) is an efficient and renowned computer windows program using an advanced tool for numerical simulation and modeling of soil media, water, heat, and solute movement in two and three-dimensional, variably saturated porous media. The program uses mass-lumped linear finite element schemes to numerically solve the Richards equation for saturated–unsaturated flow. The unsaturated soil hydraulic properties can be described using van Genuchten (1980), Brooks and Corey (1964), modified van Genuchten (Vogel and Císlerová, 1988), Durner (1994), and Kosugi (1996) type analytical functions [1]. HYDRUS was selected to model and simulate Waqf Basin in this research since (1) it was designed for simulation of recharge and infiltration of variably saturated media, (2) it utilized an extended database of soil hydraulic properties, and (3) has large and sophisticated tools for results presentation and manipulation [5]. As said, the modified version of Richards equation as explained in Richards (1931) for the two-dimensional Darcian flow of water in a variably saturated porous media is the one used in HYDRUS 2D/3D as mentioned in Celia et al. (1990) and HYDRUS (2006), Eq. (1).

$$\frac{\partial \theta}{\partial t} = \frac{\partial}{\partial x}\left(K(h)\frac{\partial h}{\partial x}\right) + \frac{\partial}{\partial z}\left(K(h)\left(\frac{\partial h}{\partial z} + 1\right)\right) \quad (1)$$

where θ is the volumetric soil water content; t is the time; h is the pressure head; x and z are coordinates, and K is the unsaturated hydraulic conductivity function [$K(h) = K_s K_r(h)$], where K_s is the saturated hydraulic conductivity and K_r is the relative hydraulic conductivity. HYDRUS graphic user interface usually follows a set of organized steps that are common to most applications. The following phases explain creating the project of Waqf Basin model until simulation.

3. Model definition and setting up

The project set up in HYDRUS 2D/3D is organized in a step-by-step procedural method that empathized the movement to the subsequent step after the full completion of the previous one adequately as explained.

- At the domain type and units, the geometry type of the transport domain (size) is defined according to the actual size, where a 3D-general type of geometry was selected for modeling the three-dimensional complex transport domain of Waqf Basin.
- Units are set in meters and the initial workspace was set to 150 m × 150 m × 40 m for x, y, and z, respectively. This defines the size of the working space depending upon the part of Waqf Basin model that was simulated.
- Only the water flow option as a main process was selected to be simulated, however, HYDRUS can simulate solute transport, heat transport, root uptake, and slope stability.
- In the time information dialog window, time unit (years, days, hours, min, sec) throughout the application was assigned in days, where in the time discretization, the initial time was set to 0 d and the final time was set to 10 d (the entire simulation time).
- In the output information dialogue window, the count of print times was set to 10 at which detailed information about the pressure heads, water contents, fluxes, and the soil water balances will be printed and analyzed.
- Iteration criteria dialog window contains information related to the iterative process that is used to solve the Richards equation. Because of the nonlinear nature of the Richards equation, an iterative process must be used to obtain solutions of the global matrix equation at each time step. For each iteration, a system of linearized algebraic equations is first derived and then solved using either Gaussian elimination or the conjugate gradient method [6]. After solving the matrix equation, the coefficients are re-evaluated using this solution, and the new equations are again solved. The iterative process continues until a satisfactory degree of convergence is obtained, which until for all nodes in the saturated (unsaturated) region, the absolute change in pressure head (or water content) between two successive iterations becomes less than some small value determined by the entered absolute pressure head (or water content) tolerance. The first estimate (at zero iteration) of the unknown pressure heads at each time step is obtained by extrapolation from the pressure head values at the previous two levels of time [6]. For this research, the maximum number of iterations was set to 100 because

of the high complexity of the 3D model, knowing that 10, 30, and 50 iterations were tested, and an error of solution convergence was encountered.
- Then, we select the soil hydraulic model for the soil hydraulic properties and specify whether hysteresis is to be considered during the calculations. HYDRUS allows the selection of six types of single porosity models for the soil hydraulic properties:
- Van Genuchten–Mualem model (van Genuchten, 1980),
- Van Genuchten–Mualem model with an air-entry value of –2 cm,
- Modified van Genuchten type equations (Vogel & Cislerova, 1988),
- Equations of Brooks and Corey (1964),
- Log normal distribution model of (Kosugi, 1996),
- Dual-porosity model (Durner, 1994).

Additionally, we can select two dual-porosity non-equilibrium flow models with mass transfer between the mobile and immobile zones assumed to be proportional to either water content or pressure head [6]. In this research, the dual porosity (mobile–immobile) for water content mass balance was selected as a soil hydraulic model since this model is accurate in calculating the mass balance of water content in the entire transport domain region with a percent error of less than 1%.

4. Model calibration and validation

The approach of model calibration and validation in HYDRUS may vary widely depending upon the complexity of the project. Model calibration and inverse parameter estimation can be carried out using a relatively simple, gradient-based, local optimization approach based on the Marquardt–Levenberg method, which is directly implemented into the HYDRUS codes, or more complex global optimization methods, including genetic algorithms, which need to be run separately from HYDRUS [7]. The program has the ability to solve two types of problems (direct and inverse problems), depending upon some specific parameters as explained.

5. Direct solution

The direct problem also referred to as forward simulation, is used when the initial and boundary conditions for all involved processes and corresponding model parameters are known. This type of solution is available for one, two, and three-dimensional transport domains. HYDRUS is a physically based model and as such requires little or no calibration when all required input parameters (soil hydraulic parameters for water flow, solute transport and reaction parameters, and thermal parameters for heat transport) are experimentally or field determined. HYDRUS has been successfully applied to laboratory and field experiments using parameters that were all determined independently of the modeling itself and hence were not calibrated [7]. Very comprehensive studies, in which all required input parameters were determined independently, were carried out by Gonçalves et al. [8] and Ramos et al. [9] and they determined soil hydraulic and solute transport parameters on laboratory columns and reaction parameters from chemical analysis, and then used HYDRUS to successfully simulate water contents, solute concentrations of individual cations, and various integral variables without calibration [7]. HYDRUS direct solution was used for Waqf Basin simulation as all related parameters of the basin were precisely determined as obtained by the study of Helles and Y. Mogheir [3,4], the observed and field data were used in this research. One important point to mention is that the three-dimensional complex transport domain such as Waqf Basin can only be solved in HYDRUS using the direct problem method as the inverse problem method is only available for one and two-dimensional transport domains.

6. Inverse solution

Inverse problems involve the estimation of selected parameters from available experimental or field data. HYDRUS under the inverse problem compares the entered field data (observed data) with the simulation results, and then the model runs several times until obtaining the parameters that emphasize the best fitting for the observed data, where this process in HYDRUS is known as a model calibration or inverse parameter estimation. Unfortunately, the inverse problem is only available in HYDRUS for one and two dimensional transport domains and not three-dimensional ones [10].

7. Model creation and simulation

After the completion of assigning the definition and information of project settings, Waqf model was created and drawn in the identified workspace area and hierarchical procedural steps were followed to complete building up the model before the final program run. The sequential steps were discussed comprehensively in the following sections as organized in Fig. 1.

8. Model geometry

Waqf Basin geometry representing the transport domain was created in HYDRUS using the available drawing tools and sets. The type of geometry was assigned as 3D-general to facilitate the creation of basin complex elements as mentioned before in model definition and setting

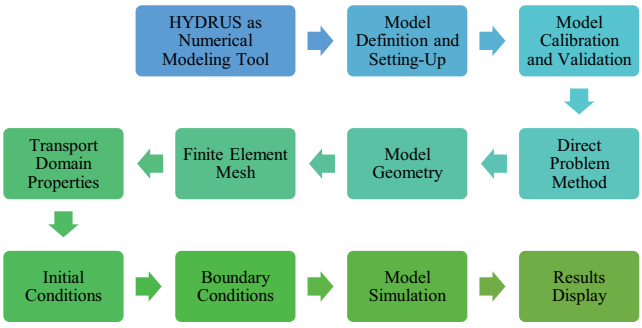

Fig. 1. Flow chart of HYDRUS steps for the creation of Waqf model.

up, particularly boreholes (drywells) that penetrate different soil layers underneath the basin floor. The bottom of Waqf Basin size was large (185 m × 70 m) in length and width, respectively, therefore, to reduce and minimize HYDRUS running time, a part of the basin was created which comprised the 18 drywells in zone 4, thus no need to model and simulate the other zones of Waqf Basin since the surface infiltration through basin floor was neglected as mentioned before, Fig. 2.

The basin model geometry was built up on a real scale, depending upon the actual layout of the basin floor and the distributed drywells in zone 4. A DXF file format was exported from AutoCAD and used in HYDRUS to aid and support drawings and design, then the two-dimensional shapes were converted into three dimensional solids using solid extrude and translate tools, Fig. 3a. The thicknesses of extruded surfaces (solids) were created according to the soil layers and profile that will be discussed in the following sections. One may notice that the bottom dimensions of the created transport domain (100 m × 120 m) were larger than the original zone 4 of Waqf Basin (50 m × 70 m) which was to mimic a sufficient soil profile for displaying the output results on the spectrum and contour plots, Fig. 3.

Fig. 3b also shows that the model geometry of Waqf Basin was created with 18 drilled boreholes which were created as filled cylindrical solid type (not hollow), thus the borehole's circular openings were filled with planar surface boundary and then extruded together with the external boundary surface. Furthermore, Fig. 4 shows that the overall depth of the drywell was 16.5 m extending down in the model domain, and only the lower 10 m of the casing UPVC pipes (0.355 m diameter) of drywells were perforated (20%–25% slotted side area), whereas the upper parts of drywells of 6.5 m were un-perforated, Fig. 4. This emphasized that the stormwater will only infiltrate through the 10 m perforated part of the drywells, which was mimicked by assigning specific materials as in the following section.

In addition, the top layer of Waqf Basin domain was created with a depth of 1.0 m to mimic the gravel gabion depth surrounding the top of boreholes UPVC casing as seen in Fig. 2b. The groundwater interface was encountered at depth of 23.5 m underneath the basin bottom (7 m beneath the boreholes ends) and was assigned in HYDRUS as discussed in the initial conditions of Waqf transport domain. In Fig. 4, the green highlighted color indicated the perforated part of the UPVC pipes (drywells) that allow stormwater to seep into soil media while the yellow highlighted color indicated the un-perforated part.

9. Finite element mesh

According to the various level of refinement for the domain elements, HYDRUS automatically creates a mesh from the model's created geometry. Numerical methods usually divide the time and spatial coordinates into smaller sections in order to obtain solutions at specific time intervals. In this way, a set of algebraic equations can be used to determine flow at each timestep in place of the continuous process that is described by partial differential equations. Most numerical techniques, including those in HYDRUS, employ time-stepping between the initial condition and the simulation final output. Finite elements (FE) are used for the solution of spatial coordinates whereas time finite differences are used for the solution of temporal equations. The FE-mesh is a discretization process in which HYDRUS splits and divides the flow transport domain (three-dimensional model geometry) into tetrahedral, hexahedral, and/or triangular prismatic three-dimensional elements (parts) that are created from the geometry nodes (joints). Where the size of the elements is determined and predefined globally for the whole domain based on the domain size and the level of accuracy required. The time discretization is performed using an implicit (backward) finite difference scheme, for (un)saturated conditions. Since this scheme is highly non-linear an iterative process is necessary to come to a solution for the global matrix equation at every time step [10].

After creating the geometrical domain of Waqf Basin, the model was divided and discretized into the FE-mesh. Since the transport domain of Waqf Basin was large (100 m width × 120 m length × 40 m height), the FE-mesh global size of the element was set to equal 2.40 m, which reduced the required module calculation time. Nonetheless, refinement of the mesh was required at some locations in the domain to create tiny sizes of mesh elements, particularly for the 18 drywells overall cylindrical solids, where the mesh element size was refined to 0.8 m to provide accurate analysis results and fulfill the smoothness criterion, Figs. 5 and 6 show the discretization of Waqf Basin model into generated mesh elements.

Table 1 displays the information on the created FE-mesh of Waqf Basin; the information shows the statistics of global mesh with mesh refinement of the 18 boreholes.

The mass balance error that HYDRUS reported at the end of the simulation, shows the accuracy of the finite element mesh that was generated. For an acceptable accuracy, mass balance errors should always be less than 1%.

10. Domain properties

The soil layers were assigned to the geometrical domain of Waf basin model, and the soil properties were obtained based on geotechnical testing results of soil layers underneath the basin floor as shown in Fig. 7.

The spatial distribution of the domain properties on Waqf Basin model varies in space and can be defined on geometrically created solids or directly on the created finite element mesh. Five soil types were created as shown in Fig. 8a and b, the thickness of each soil layer was assigned in a different color, starting from the upper boundary of the transport domain. A gravel layer of 1.0 m thick with hydraulic conductivity K_s = 14.48 m/d was assigned at the top of the transport domain to mimic the graveled gabion cubes which were surrounding the caps of the 18 constructed boreholes with a height of 1.0 above the surface of the basin bottom. The ponded stormwater height in Waqf Basin was assigned to the upper surface of this created layer of graveled gabion as explained in the following sections of boundary conditions.

Then, a clay soil layer of 6.5 m thick was defined in the transport domain as seen in Fig. 8, this will mimic the un-perforated parts of drywells UPVC casing pipes to assure that stormwater will seep and infiltrate through only

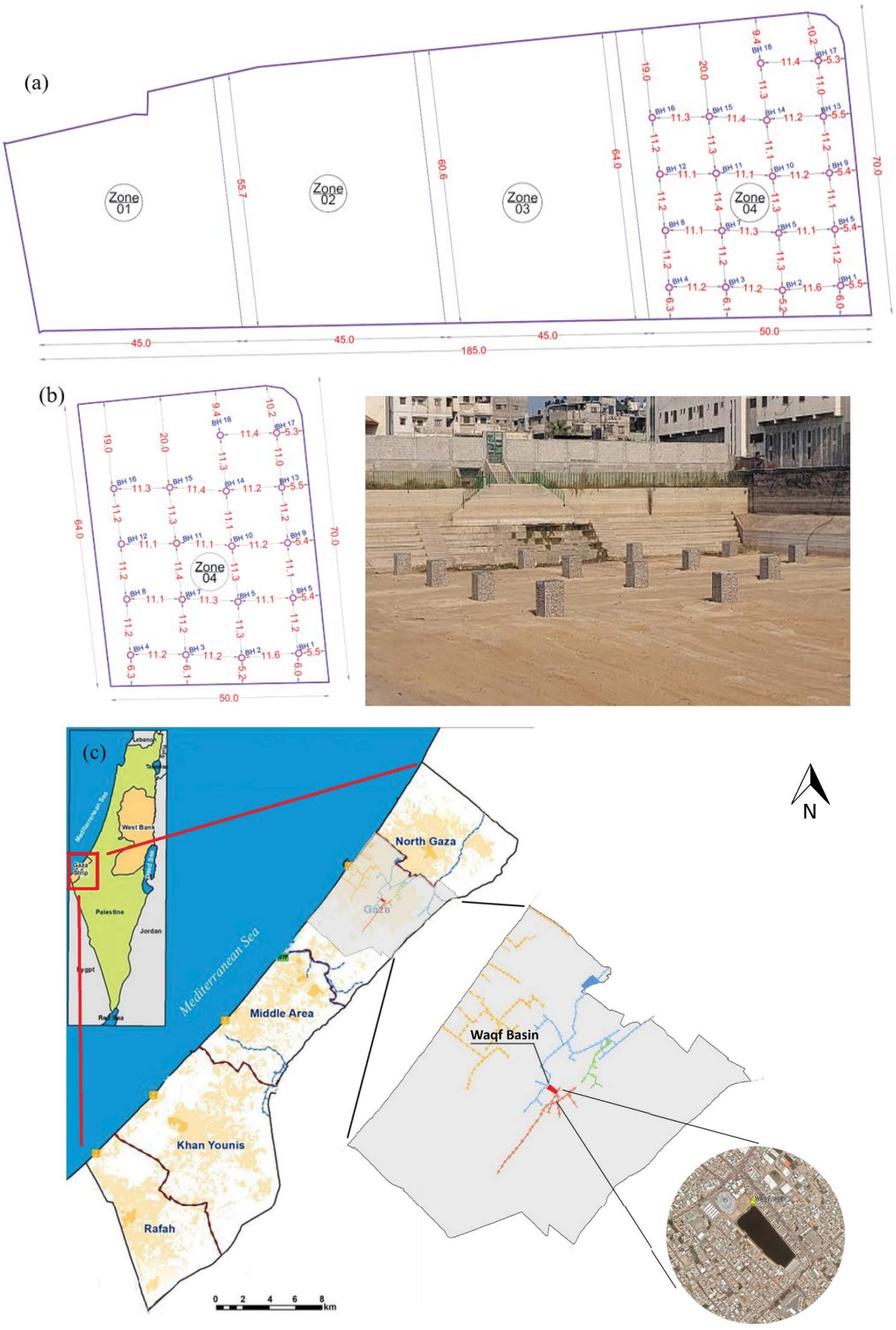

Fig. 2. Layout of Waqf Basin: entire basin layout (a), modeled part of zone 4 (b), Waqf Basin map (c).

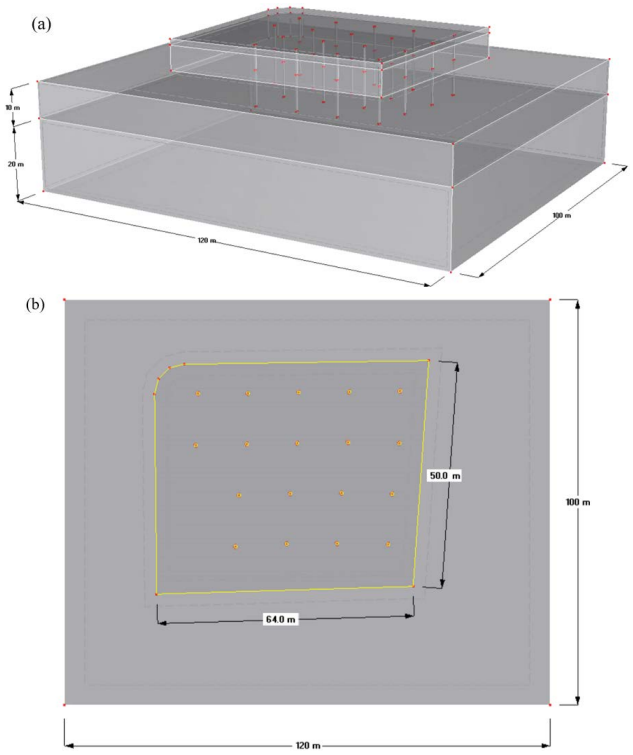

Fig. 3. Geometry of Waqf model: isometric view (a), top view (b).

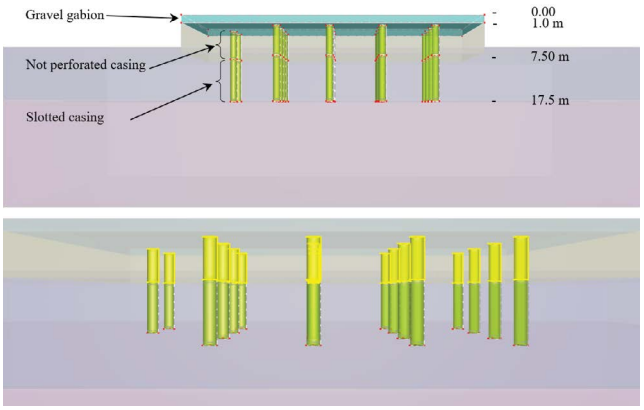

Fig. 4. Boreholes geometrical details of Waqf Basin domain.

the perforated parts (10 m high) of drywells casing pipes. The clay material was selected owing to its poor permeability and low hydraulic conductivity K_s = 0.048 m/d, which was obtained by the HYDRUS soil catalog of predefined soil hydraulic properties for well-known soil materials as studied by Šimůnek et al. [10] and Schaap et al. [11]. In addition, defining the clay material as a top layer of the transport domain, assured that collected stormwater will not seep and infiltrate through the basin floor surface but rather would only do so through the 18 drilled boreholes. As illustrated in previous sections, the boreholes were created as cylindrical geometrical shapes (cylindrical solids) that extend in clay and coarse sand layers until reaching the bottom of the coarse sand layer (top of the kurkar layer).

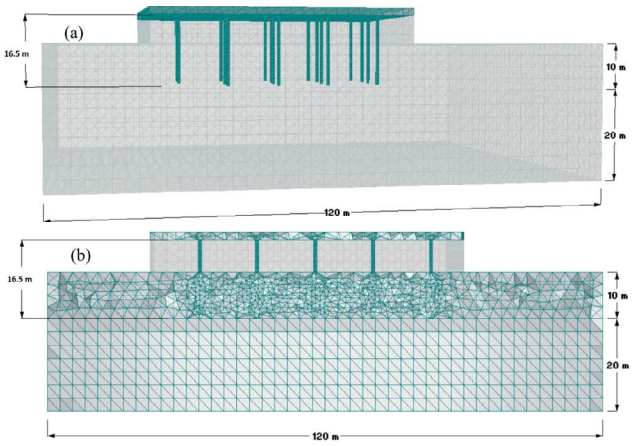

Fig. 5. Sections displaying the FE-mesh at Waqf Basin model (a), and (b).

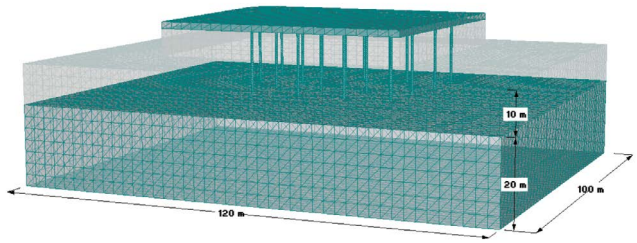

Fig. 6. Isometric display of FE-mesh of Waqf Basin model with 18 drywells.

Table 1
FE-mesh statistics of Waqf Basin model

FE-M information	Number/size
Nodes	73,577
1D-Elements	1,647
2D-Elements	21,364
3D-Elements	410,865
Type of 3D elements	Tetrahedral
Max. number of nodes	200,000
Targeted FEM size (m)	2.40
Mesh refinement size (m)	0.80

To mimic the actual situation of boreholes being non-backfilled with any media, a gravel material of very high hydraulic conductivity K_s was assigned to the borehole's solids. HYDRUS soil catalog defines the loamy sand material K_s as 3.502 m/d, then by trial and error, we increased this loamy sand K_s by about 100 times to identify a potential gravel K_s as 3.502 m/d, which was assigned to all borehole's solids.

The coarse sand layer that has a thickness of 10 m and surrounds the perforated parts of the 18 drywells was assigned to a hydraulic conductivity K_s of 24.50 m/d, (average of 22.64 to 26.35 m/d based on geotechnical testing results). The lowest domain soil layer of 20 m thick was assigned

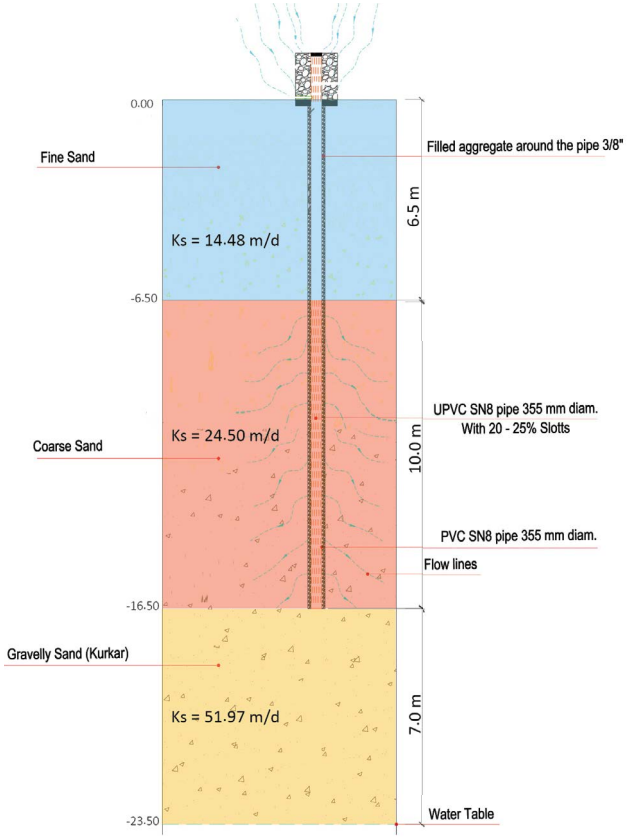

Fig. 7. Soil profile with assigned K_s for underlying layers.

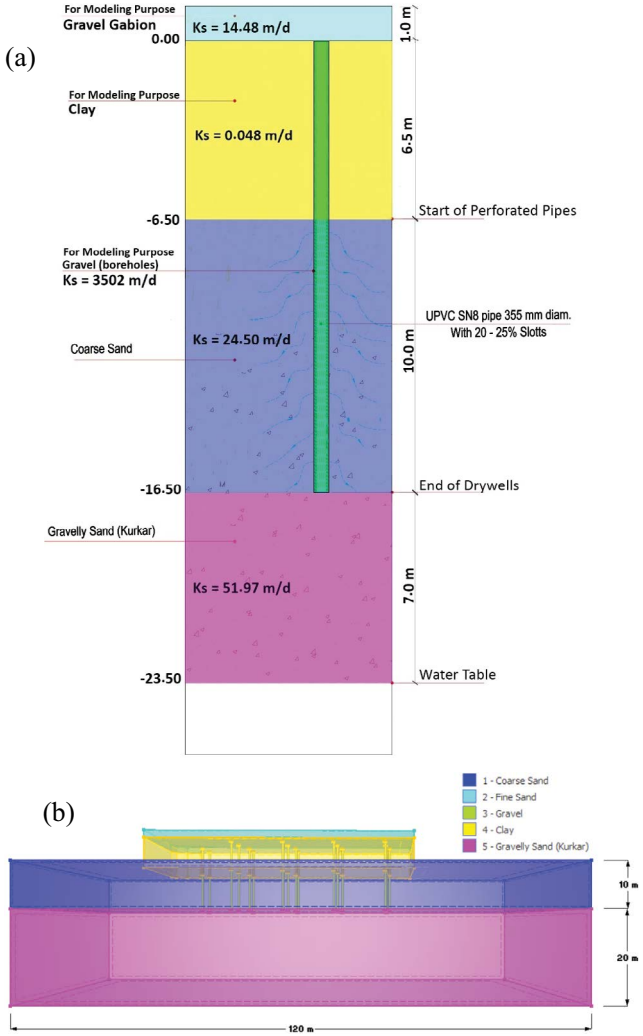

Fig. 8. Soil layers assigned with corresponding K_s: layered soil profile (a), transport domain properties of Waqf Basin (b).

with kurkar material that has a hydraulic conductivity K_s of 51.97 m/d (average of 28.43–75.51 m/d based on geotechnical testing results). The kurkar layer comprised the groundwater table as will be discussed in the following section of initial conditions, through which stormwater infiltrated deeply into the soil media as displayed by the water movement and flowlines after the program running time. Table 2 presents the soil layers information that was entered in HYDRUS as domain properties for Waqf Basin.

The soil hydraulic parameters in Table 2 were defined based on the selected soil hydraulic model (mobile–immobile, water mass transfer) as discussed in previous sections. In this model, both Q_r and Q_s denote the residual and saturated water contents, respectively; K_s is the saturated hydraulic conductivity, and l is a pore-connectivity (tortuosity) parameter. The parameters α (Alpha) and n are empirical coefficients affecting the shape of the hydraulic functions. We may select from a catalog of several soil types with varying soil hydraulic characteristics in HYDRUS to allocate the material to a particular part of the domain. For the van Genuchten model, the parameters were taken from van Genuchten [12], while for the Brooks–Corey model, they were taken from Carsel and Parrish [13]. Furthermore, the soil hydraulic properties catalog in HYDRUS was predicted using neural network analysis of hierarchical prediction which comprised the following twelve soil textural classes (using the classification based on the USDA textural triangle) [10], as shown in Table 3.

Table 2
Domain properties of Waqf Basin model, from (van Genuchten [12])

Soil name	Q_r (–)	Q_s (–)	α (1/m)	n (–)	K_s (m/d)	I (–)
Fine sand	0.045	0.43	14.5	2.68	14.48	0.5
Clay	0.068	0.38	0.80	1.09	0.048	0.5
Coarse sand	0.057	0.41	3	1.5	24.50	0.5
Gravelly sand (kurkar)	0.057	0.41	3	1.5	51.97	0.5
Gravel (boreholes)	0.057	0.41	3	1.5	3,502.0	0.5

11. Initial conditions

The initial condition is used to specify the status of the entire transport domain at the beginning of the model simulation based on each considered process. HYDRUS can

assign two controllers for the initial condition of a transport domain; one can specify whether the initial condition for the water flow calculations is to be specified in terms of pressure head or water content. While the pressure head initial condition is available in HYDRUS with three types of distribution, the water content initial condition is only available with two. The following are three types of distribution for the pressure head initial condition that were assigned in this research [13]:

- Constant: homogenous distribution of water content or water pressure head over the entire soil profile, negative values indicate a negative pressure head and a dry domain (very deep water table), while positive values indicate a wet domain.
- Linear distribution with depth: This indicates that the top and bottom pressure heads are set with specific values, with a linear distribution in between.
- Equilibrium from the lowest local nodal point: which indicates that only the bottom pressure head condition is set, and equilibrium conditions are applied to the soil above, this option was selected for this research. The positive value indicates that the water table is located above the lowest local nodal point of the domain, and if assigned zero this indicates that the water table is located at the lowest local nodal point of the transport domain.

Since the pressure head values (ponded water levels) and water table location are well known as investigated by Helles and Mogheir [3], Waqf Basin model was set to be controlled by the pressure head initial condition rather than the water content initial condition. As stated, the distribution of pressure head initial condition was selected as equilibrium from the lowest located nodal point (lowest z-coordinate elevated point in the geometry), since this option allows to specify the location of the water table based on the lowest point in the transport domain. The water table was encountered in the field at 23.5 m underneath the ground surface.

Table 3
Soil hydraulic properties of 11 soil classes in HYDRUS [14]

Soil name	Q_r (–)	Q_s (–)	α (1/m)	n (–)	K_s (m/d)	I (–)
Sand	0.045	0.43	14.5	2.68	7.128	0.5
Loamy sand	0.057	0.41	12.4	2.28	3.502	0.5
Sandy loam	0.065	0.41	7.5	1.89	1.061	0.5
Loam	0.078	0.43	3.6	1.56	0.2496	0.5
Silt	0.034	0.46	1.6	1.37	0.06	0.5
Silty loam	0.067	0.45	2	1.41	0.108	0.5
Sandy clay loam	0.1	0.39	5.9	1.48	0.3144	0.5
Clay loam	0.095	0.41	1.9	1.31	0.0624	0.5
Silty clay loam	0.089	0.43	1	1.23	0.0168	0.5
Sandy clay	0.1	0.38	2.7	1.23	0.0288	0.5
Silty clay	0.07	0.36	0.5	1.09	0.0048	0.5
Clay	0.068	0.38	0.8	1.09	0.048	0.5

To mimic this in HYDRUS, the value of the bottom pressure head initial condition was obtained as expressed in Eq. (2).

$$\text{Perched water table}(m) = \text{Domain thickness} - (\text{Lowest local nodal point}) \quad (2)$$

$$23.5(m) = (6.5 + 10.0 + 20.0) - (X)$$

X = 36.5–23.5 = 13.0 m, thus, we enter the positive value of 13.0 m for the option of equilibrium from the lowest local nodal point to locate the water table in the transport domain of Waqf Basin, Fig. 9.

Furthermore, the pressure head equals zero (atmospheric pressure) at the groundwater table interface, which separates the fully saturated soil (below) from the variably saturated soil (above). As a result of soil partial saturation, negative pressure (also known as a suction head or matric potential), which is lower than the atmospheric pressure is encountered above the water table.

12. Boundary conditions

On the other hand, the boundary conditions are sets of controllers that describe the situation and determine the flow of water through the geometrical domain boundaries, informing HYDRUS what is occurring at the external domain boundaries. Depending on the problem, we can in HYDRUS assign various types of boundary conditions, such as free seepage, deep/free drainage, no-flux, constant head, constant flux, and others. The constant head boundary condition was selected with three pressure head values of 1.70, 3.40, and 5.10 m and was assigned to the top surface of the transport domain (colored in red), Fig. 10. Three scenarios of ponded water depth (1.70, 3.40, and 5.10 m) were studied in HYDRUS as different boundary conditions that provided different values of water flux to the transport

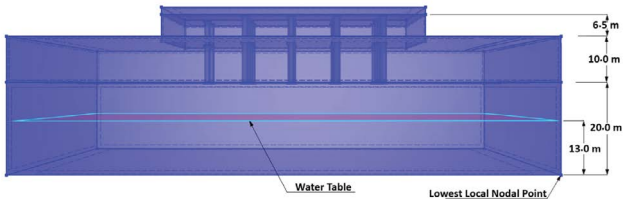

Fig. 9. Water table underneath Waqf Basin model in HYDRUS.

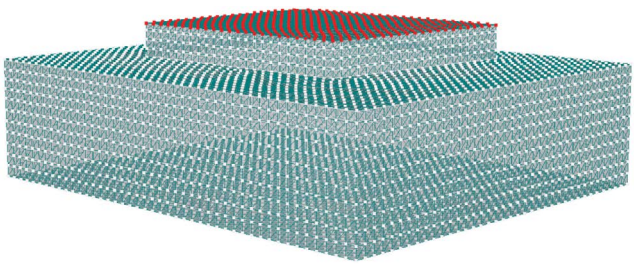

Fig. 10. Boundary conditions assigned to Waqf Basin model in FE-mesh mode.

domain. Each particular scenario mimicked a constant ponded water depth in Waqf Basin, with an entire HYDRUS calculation time of 10 d for each scenario. The water depth was assigned to the sand layer top surface (graveled gabion) that has a depth of 1.0 m in Waqf Basin model. The different water depth scenarios in HYDRUS have developed important results that were studied and compared to the results of field observation readings obtained during the 2021–2022 wet seasons. The other transport domain boundaries were set to no-flux boundary condition (colored in white), as shown in Fig. 10.

Thus, the stormwater seeped and infiltrated into sublayers through the green colored part of the borehole cylindrical solids which represents the lower 10 m perforated length of the casing UPVC pipes with 20%–25% slotted side area, Fig. 11.

13. Results and outputs

The HYDRUS running time of Waqf model calculation was completed after around 11.0 d for each assigned scenario of constant pressure head (1.70, 3.40, 5.10 m). Then, various outputs became available for display, either graphically on the information viewport such as water content, pressure head, and velocity. However, using *x*–*y* graphs for boundary fluxes, cumulative fluxes, and mass balance information can be available. The graphical outputs of water velocity (m/d) into Waqf transport domain are shown in Figs. 12–14 at different ponded water depths using the contour colormap display mode. The color spectrum presentation with the corresponding color key index was displayed at different print times *t* (1, 5, and 10 d) of HYDRUS execution.

The water content of Waqf transport domain was also displayed at different ponded water depths in Figs. 15–17 at different print times *t* (1, 5, and 10 d) using color spectrum presentation and key indexing.

The pressure head of Waqf transport domain was also presented at different ponded water depths in Figs. 18–20 showing that the negative pressure of the unsaturated zone was located above the level of boreholes. The contour plot also displayed the groundwater mounding underneath the infiltration basin at different print times *t* (1, 5, and 10 d).

Other information on the borehole infiltration capacity can be obtained from the HYDRUS mass balance report as shown in Table 4. Table 4 shows that HYDRUS keeps track of the mass balance and provides results at different print times of 10 d of simulation. We can identify the total mass balance of the model from the information obtained in the HYDRUS output balance report. In some cases, the transport domain can be subdivided into subregions to display the results of each particular layer of the model. However, in this research one region was applied to avoid long computational running time. The amount of water stored in Waqf model transport domain varied based on both the time and the depth of ponded stormwater. At the print time $t = 0$ for the ponded water depths 1.70, 3.40, and 5.10 m, the model gave the same amount of stored water in the transport domain estimated as 97,520.0 m^3, whereas the amount of stored water at the print time $t = 10$ varied based on the corresponding ponded water depths 1.70, 3.40, and 5.10 m and was obtained as 149,630.10, 156,415.50, and 160,590.0 m^3, respectively. Also, it is important to notice that the percent error $Wat_{Bal\ R}$ was less than 1% in the three cases of ponded water depths, which indicated an accepted accuracy of model computation for the three scenarios.

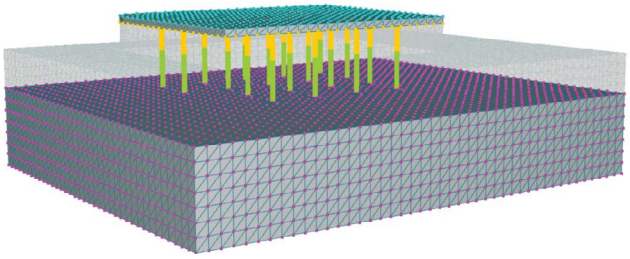

Fig. 11. Infiltrating part of the recharge boreholes (green perforated parts) in FE-mesh mode.

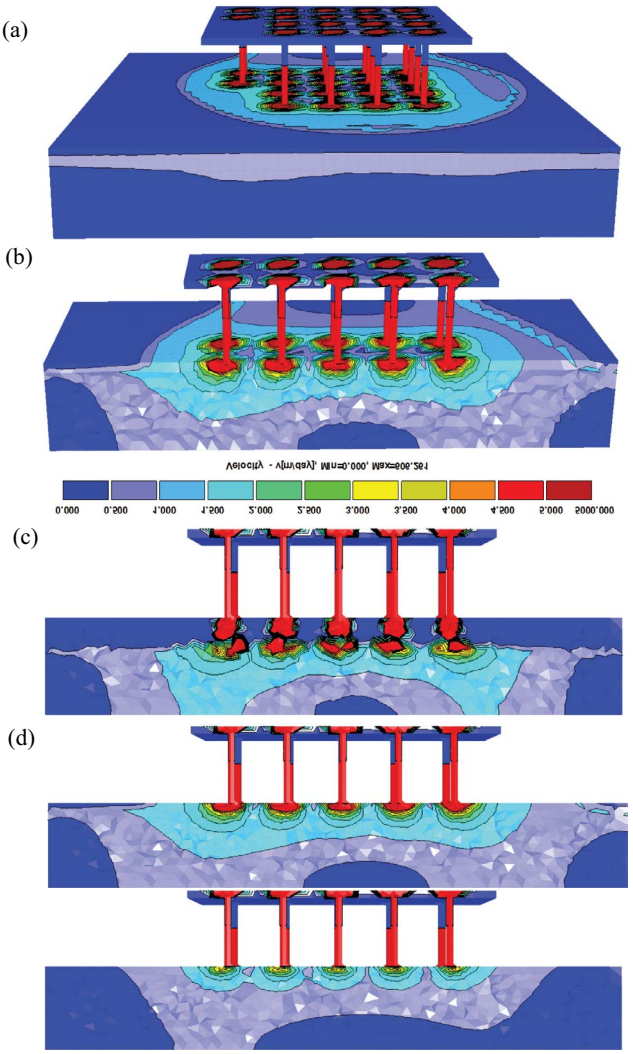

Fig. 12. Velocity of water flow in Waqf Basin domain at 1.70 m ponded water depth: isometric shape of entire domain (a), domain section displaying boreholes (b), velocity of flow at $t = 1$ d (c), at $t = 5$ d (d), at $t = 10$ d (e).

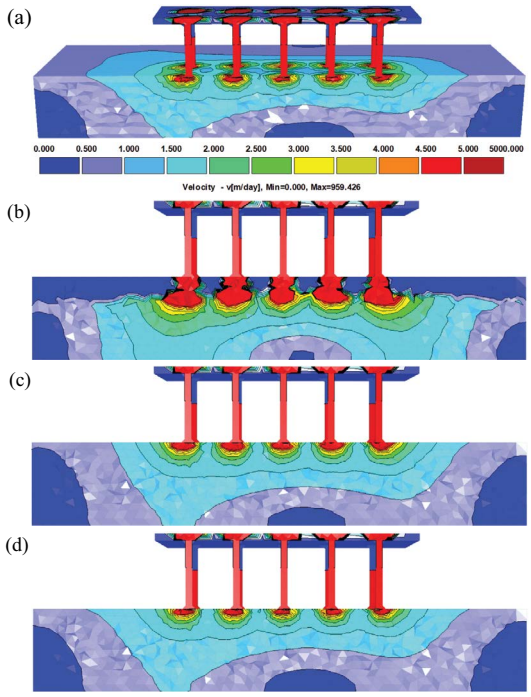

Fig. 13. Velocity of water flow in Waqf Basin domain at 3.40 m ponded water depth: isometric shape of entire domain (a), velocity of flow at t = 1 d (b), at t = 5 d (c), at t = 10 d (d).

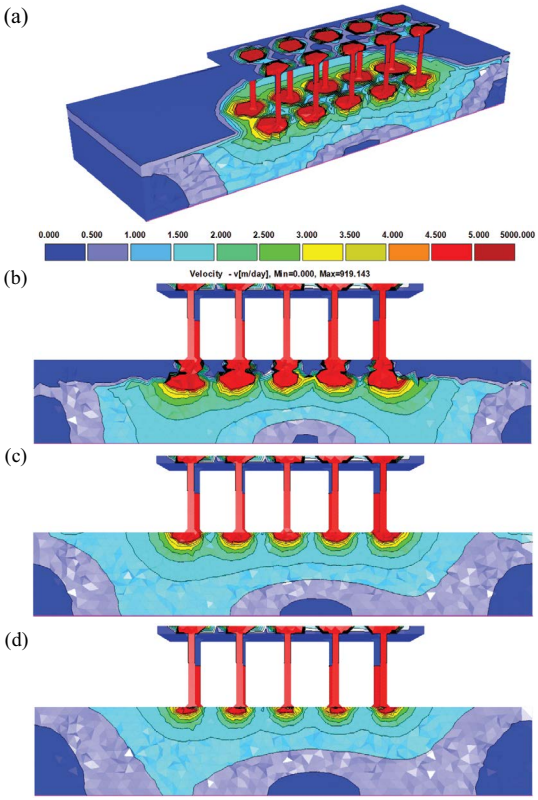

Fig. 14. Velocity of water flow in Waqf Basin domain at 5.10 m ponded water depth: isometric shape of entire domain (a), velocity of flow at t = 1 d (b), at t = 5 d (c), at t = 10 d (d).

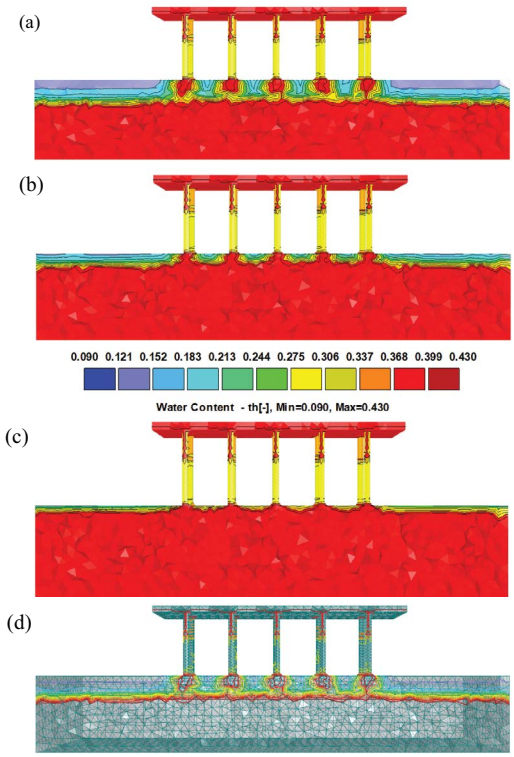

Fig. 15. Water content display of Waqf Basin at 1.70 m ponded water depth: at t = 1 d (a), at t = 5 d (b), at t = 10 d (c), at t = 10 d using isolines display (d).

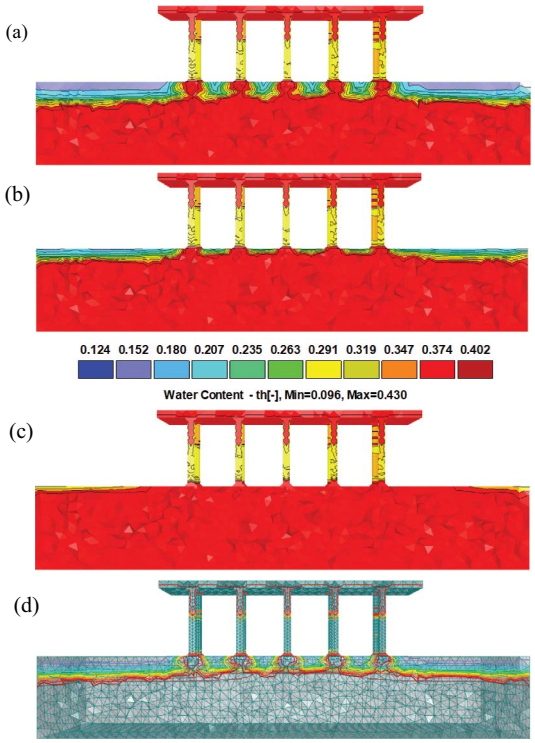

Fig. 16. Water content display of Waqf Basin at 3.40 m ponded water depth: at t = 1 d (a), at t = 5 d (b), at t = 10 d (c), at t = 10 d using isolines display (d).

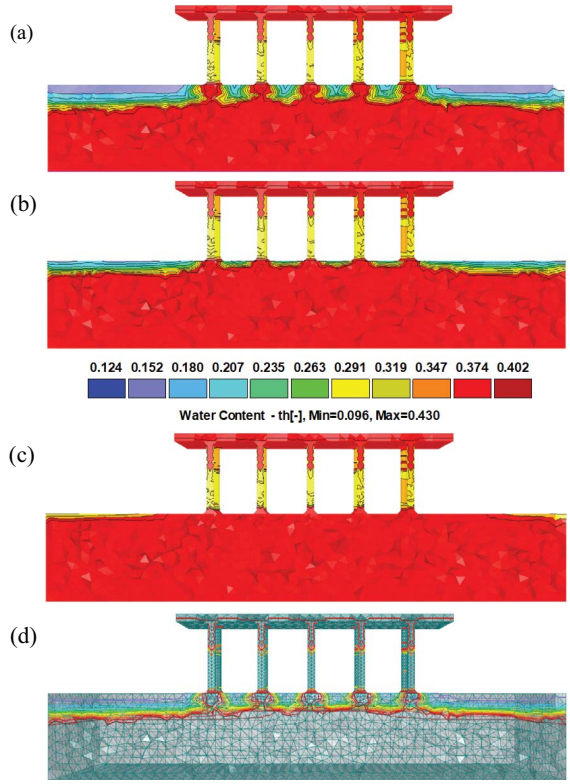

Fig. 17. Water content display of Waqf Basin at 5.10 m ponded water depth: at t = 1 d (a), at t = 5 d (b), at t = 10 d (c), at t = 10 d using isolines display (d).

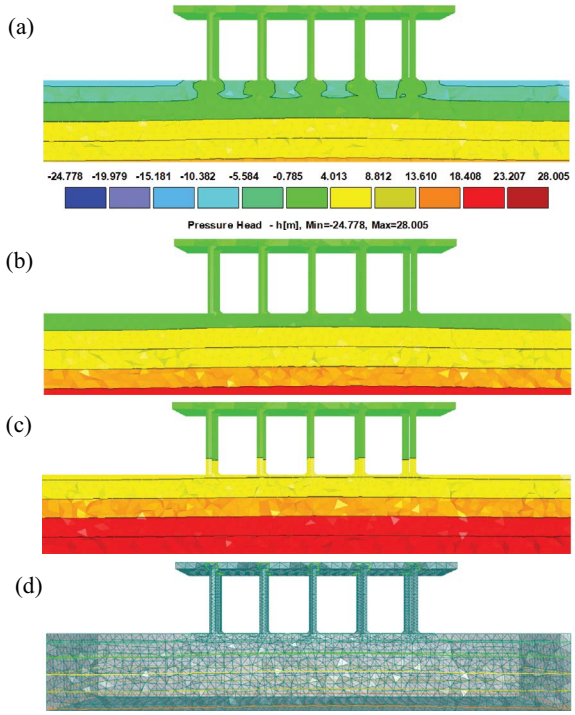

Fig. 18. Pressure head display of Waqf Basin at 1.70 m ponded water depth: at t = 1 d (a), at t = 5 d (b), at t = 10 d (c), at t = 10 d using isolines display (d).

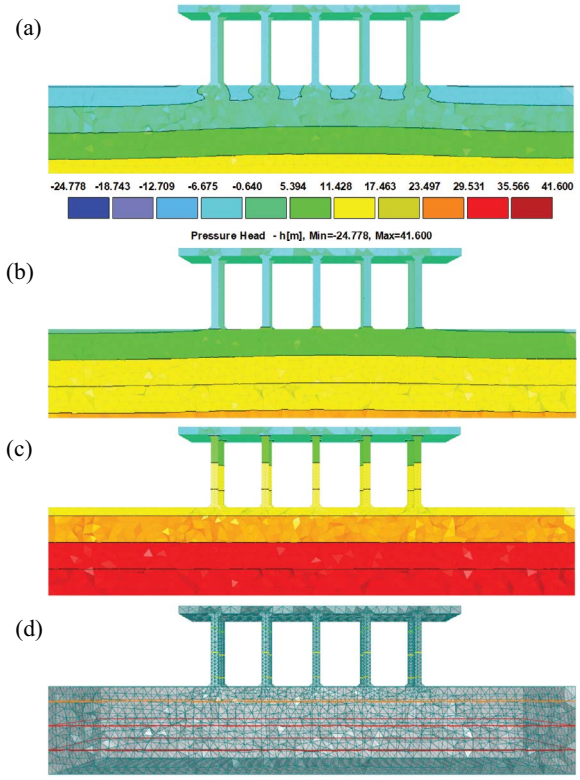

Fig. 19. Pressure head display of Waqf Basin at 3.40 m ponded water depth: at t = 1 d (a), at t = 5 d (b), at t = 10 d (c), at t = 10 d using isolines display (d).

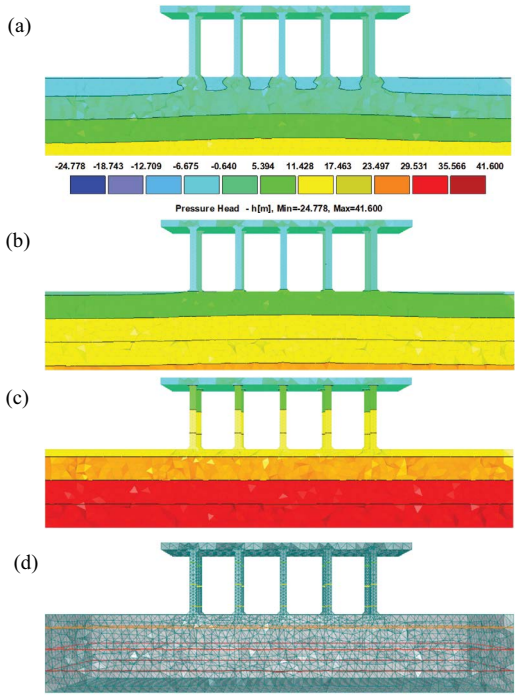

Fig. 20. Pressure head display of Waqf Basin at 5.10 m ponded water depth: at t = 1 d (a), at t = 5 d (b), at t = 10 d (c), at t = 10 d using iso-surfaces display (d).

Table 4
HYDRUS mass balance information at different ponded water depths

HYDRUS item	h_{ponded} = 1.70 m		h_{ponded} = 3.40 m		h_{ponded} = 5.10 m		Description
	t = 0 d	t = 10 d	t = 0 d	t = 10 d	t = 0 d	t = 10 d	
Volume (m^3)			386,220.0				Size of the transport domain
Volume $_W$ (m^3)	97,520.0	149,630.1	97,520.0	156,415.0	97,520.0	160,590.0	Volume of stored water
Volume $_{Im}$ (m^3)			21,322.0				Volume of immobile water content
Inflow (m^3/d)	0.0	4,392.1	0.0	4,440.0	0.0	4,612.0	Inflow and outflow fluxes
h_{Mean} (m)	–3.13	11.80	–0.98	15.5	–1.0	17.3	Mean pressure heads
Wat $_{Bal\ T}$ (m^3)	0.0	–107.5	0.0	–113.56	0.0	–117.84	Absolute error in the water mass balance
Wat $_{Bal\ R}$ (%)	0.0	0.20	0.0	0.19	0.0	0.15	Relative error in the water mass balance
Running time (d)	0.0	10.96	0.0	17.87	0.0	19.0	Simulation period

14. Results discussion

Three scenarios of the ponded water depths (1.70, 3.40, and 5.10 m) were assigned in HYDRUS and results were obtained and displayed. The results presented the volume of stormwater stored in the transport domain during the model running time (10 d) at each ponded water depth. Then, a comparison was created to identify the variation that occurred in the borehole infiltration capacity. The difference in the volume of water stored in the transport domain between print times of 0 and 10 d was calculated using Eq. (3).

$$\text{Change in Storage}\left(\text{m}^3\right) = \text{Volume}_{(\text{at},10\text{ days})} - \text{Volume}_{(\text{at},0\text{ days})} \quad (3)$$

We substitute the obtained values from HYDRUS mass balance report at each ponded water depth into Eq. (3) to get the results shown in Table 5.

Table 5 illustrates the total infiltrated volume of stormwater into Waqf Basin transport domain after the 10 d of model simulation for the three different ponded water depths. The infiltration capacity of Waqf Basin was calculated in Table 6 by dividing the total infiltrated volume of stormwater by the 10 d of simulation at each ponded water depth which was then divided by the number of existing boreholes (18 boreholes) to obtain the average single borehole infiltration capacity at each ponded water depth.

One may notice, the average borehole infiltration capacity over the 10 d of simulation time was calculated as 289.5, 327.2, and 350.39 m^3/d for the ponded water depths of 1.70, 3.40, and 5.10 m, respectively. However, as shown in Table 7, HYDRUS can estimate the real borehole infiltration capacity on each simulated day for the various ponded water depths.

At 1.70 m ponded water depth, the borehole infiltration capacity was declining over the simulation time in an exponential regression function with a coefficient of determination R^2 equals 0.97. When the ponded water depth in Waqf Basin increased to 3.4 m, the borehole infiltration capacity increased but still declining over time in an exponential regression function with an R^2 of 0.97, the same for the 5.1 m ponded water depth but with an R^2 of 0.98. The three curves of borehole infiltration capacity during the 10 d of simulation were superimposed in a plot as shown in Fig. 21.

Table 5
Domain water storage at different ponded water depths

Ponded water depth, m	Water volume, m^3		Change in storage, m^3
	t = 0 d	t = 10 d	
1.70 m	97,520.0	149,630.1	52,110.10
3.40 m		156,415.5	58,895.00
5.10 m		160,590.0	63,070.00

Table 6
Average borehole infiltration capacity at different ponded water depths

Item	Ponded water depth, h_{ponded}		
	1.70 m	3.40 m	5.10 m
Infiltrated volume, 10 d (m^3)	52,110.10	58,895.50	63,070.00
Simulation time, (d)		10	
Daily infiltration capacity, (m^3/d)	5,211.0	5,889.5	6,307.0
No. of boreholes		18	
Average borehole infiltration capacity, (m^3/d)	289.50	327.2	350.39

On the other hand, HYDRUS also calculated the cumulative inflow amount that infiltrated and stored into the transport domain on each simulation day for different ponded water depths as presented in Table 8.

Fig. 22 shows a gradual increase in the cumulative infiltrated water over the 10 d of simulation at the three ponded water depths. Best regression was applied for the created curves using power functions. At the 1.70 m ponded water depth, the infiltrated volume increased over time with an R^2 of 1.0, and a total infiltrated water volume of 52,110.1 m^3. Whereas, when the ponded water depth increased to 3.40 and 5.10 m, the total infiltrated water volume was 58,895.0 and 63,070.0 m^3 with a corresponding R^2 of 0.99 for both. Furthermore, the cumulative inflow stored in the transport domain can be determined using another tool in HYDRUS referred to as the cumulative constant head boundary flux that gave equivalent results.

Table 7
Single borehole infiltration capacity at different ponded water depths

Time (d)	Single borehole infiltration capacity (m^3/d)		
	Ponded water depth, h_{ponded}		
	1.70 m	3.40 m	5.10 m
1	366.9	402.1	438.4
2	339.7	392.2	418.2
3	320.3	383.3	409.3
4	303.1	363.9	389.9
5	287.3	347.7	357.3
6	279.7	322.8	348.8
7	259.7	294.9	320.9
8	249.6	266.7	287.1
9	244.7	251.7	277.7
10	244.0	246.7	256.2

Table 8
Cumulative infiltrated inflow at different ponded water depths

Time (d)	Cumulative borehole infiltration capacity (m^3/d)		
	Ponded water depth, h_{ponded}		
	1.70 m	3.40 m	5.10 m
1	6,604.1	7,238.0	7,891.0
2	12,719.2	14,298.0	15,419.0
3	18,484.3	21,198.0	22,787.0
4	23,939.4	27,748.0	29,805.0
5	29,110.6	34,006.0	36,237.0
6	34,145.7	39,816.0	42,515.0
7	38,819.8	45,125.0	48,292.0
8	43,312.9	49,925.0	53,460.0
9	47,718.0	54,455.0	58,458.0
10	52,110.1	58,895.0	63,070.0

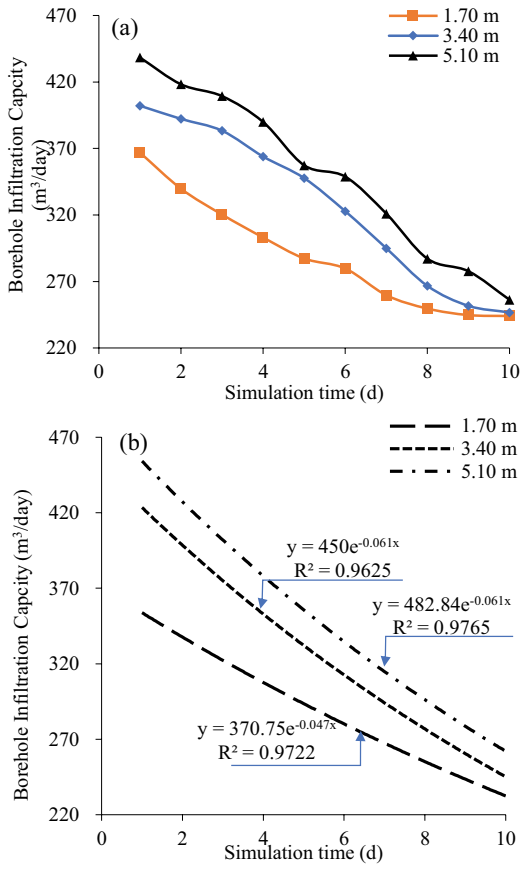

Fig. 21. Infiltration capacity over 10 d at different ponded water depths: single borehole infiltration capacity (a), best regression function (b).

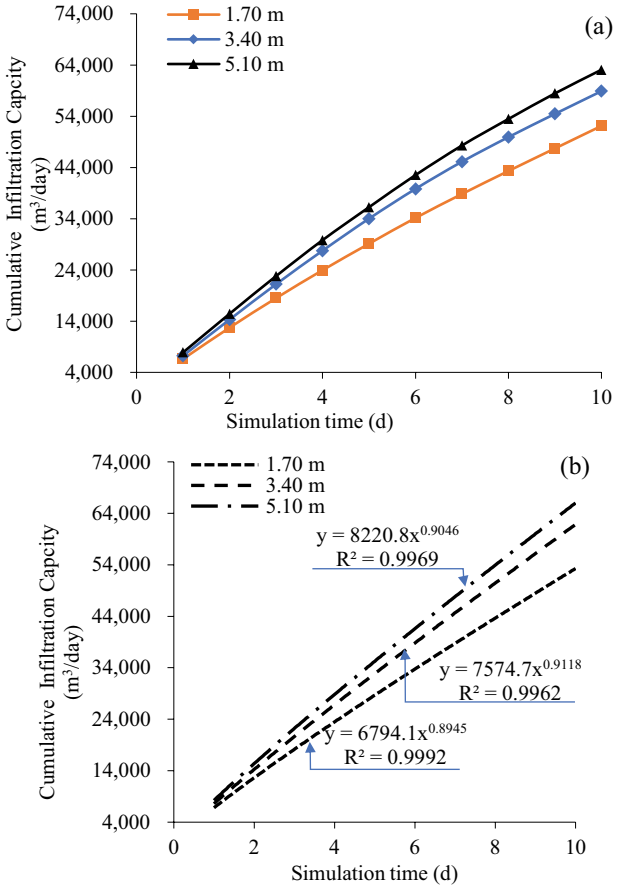

Fig. 22. Cumulative infiltrated water over 10 d: cumulative infiltration capacity (a), best regression function (b).

In addition, we compared the average single borehole infiltration capacity of the three ponded water depths using HYDRUS with the field observation readings of Waqf Basin water levels during the 2021–2022 wet season as shown in Table 9.

The HYDRUS numerical solution of borehole infiltration capacity was plotted in Fig. 23 vs. the corresponding ponded water depths and compared with the results obtained through field observed data during the 2021–2022 wet season. One may notice that there was a difference between

Table 9
Borehole infiltration capacity at different ponded water depths

Ponded water depth d_{ponded}, (m)	Single borehole infiltration capacity, (m^3/d)	
	Field observed Q	HYDRUS Q
5.10	316.7	350.39
3.40	250.0	327.19
1.70	111.1	289.0

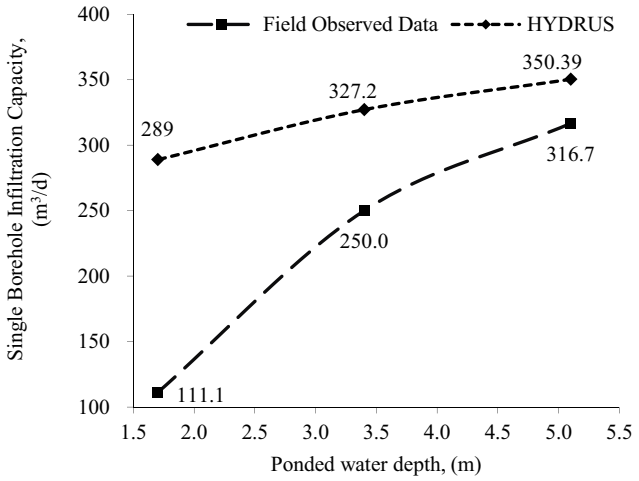

Fig. 23. Borehole infiltration capacity with respect to ponded water depth.

the two results, HYDRUS results were greater than of field observed results. In addition, the infiltration capacity of a borehole increases with the increase of the water level in the infiltration basin, and the rate of the increase varied according to the results of either HYDRUS or field observation.

The difference between results was attributed to the fact that HYDRUS has the option to simulate clogging using a tool referred to as the time variable scaling factor that decreases exponentially with time but unfortunately, this time dependent scaling factor is embodied only in HYDRUS 2-D, not 3-D version, as expressed in Eq. (4).

$$K_{s,t} = K_{s,\text{initial}} e^{-\lambda t} \tag{4}$$

where $K_{s,t}$ is the saturated hydraulic conductivity at time t, $K_{s,\text{initial}}$ is the initial saturated hydraulic conductivity, and λ is the hydraulic conductivity reducing parameter ($\lambda \geq 0$), also referred to as the clogging factor [15]. Moreover, Eq. (4) depends only on the soil characteristics ignoring the quality of the incoming stormwater, thus the equation is a simple representation of the reduction in infiltration rate over time but may not apply to all managed recharge systems. That means, the effect of the physical clogging was not considered in the HYDRUS obtained values of borehole infiltration capacity in Table 9. Thus, we can expect an equation to represent the clogging factor comparing the field readings vs. the HYDRUS values as in Eq. (5).

$$f_{\text{clogging}} = 1 - \frac{Q_{\text{Field}}}{Q_{\text{Hydrus}}} \tag{5}$$

As expressed in Eq. (5), f_{clogging} is a time dependent reducing factor that mainly varies with respect to time, ponded water depth, and soil hydraulic properties. This clogging factor can be used later to upgrade the well-known Zanager equation which is used for the design of infiltrating boreholes.

15. Conclusion

Applying the stormwater infiltration technique with augmenting boreholes (drywells) in the Gaza Strip is efficient since the technique accelerates the stormwater infiltration rate, with no risk to the groundwater quality, adding to no need for large surface areas, however, the technique needs to be carefully planned and implemented since the boreholes could become permanently clogged and backwashing might not be able to fix the problem. Thus, periodic repairs and checkups must be available at the end of every wet season. HYDRUS (2D/3D) software was used in this research to model and simulate Waqf Basin at three different ponded water depths of 1.70, 3.40, and 5.10 m. The obtained results showed that the infiltration capacity of the system and thus the single borehole infiltration capacity was in agreement with the field observed data obtained during the 2021–2022 wet season, that the borehole infiltration capacity increases with the increase of ponded water depth in the infiltration basin with a power function best regression.

The modeling/simulation approach of Waqf Basin using HYDRUS can be effectively utilized for the thorough understanding of the stormwater infiltration basin and the water flow behavior, with more emphasis on the best practice design and functionality. It is strongly recommended to incorporate the varying water level in order to achieve the best results reflecting the actual situation of the ponded water depth. For future studies, the inverse problem can be considered for Waqf Basin model as a 1D or 2D model to validate and calibrate the assigned varying ponded water depths during the simulation time rather than being constant water depths, and the effect of clogging should be considered and investigated as well. Local government officials in the Gaza Strip should focus their efforts on creating a master management plan for the overall water resources as well as exploring more innovative ideas for building advanced artificial infiltration systems that take into account new concepts and techniques and conducting in depth research to find the most suitable location for these recharge structures.

References

[1] Coastal Municipalities Water Utility (CMWU), Information Sheet of all Water Infiltration Facilities in Gaza, Unpublished Report, Gaza Strip, Palestine, 2022.
[2] J. Simunek, M. Th Van Genuchten, M. Sejna, The HYDRUS-1D Software Package for Simulating the One-Dimensional Movement of Water, Heat, and Multiple Solutes in Variably-Saturated Media, University of California-Riverside Research Reports, 2005, pp. 1–240.
[3] Z. Helles, Y. Mogheir, Assessment of stormwater infiltration basins models developed in Gaza Strip, J. Eng. Res. Technol., 9 (2022).
[4] Z. Helles, Y. Mogheir, Factors affecting the infiltration rate of stormwater (case study: three large stormwater infiltration basins in the Gaza Strip), Technix Int. J. Eng. Res. (TIJER), 9 (2022) 72–85.

[5] M. Nimmer, A.M. Thompson, D. Misra, Water table mounding beneath stormwater infiltration basins, Environ. Eng. Geosci., 15 (2009) 67–79.
[6] J. Šimůnek, M. Th. van Genuchten, Modeling nonequilibrium flow and transport processes using HYDRUS, Vadose Zone J., 7 (2008) 782–797.
[7] J. Šimůnek, M. Th. van Genuchten, M. Šejna, HYDRUS: model use, calibration, and validation, Trans. ASABE, 55 (2012) 1261–1274.
[8] M.C. Gonçalves, J. Šimůnek, T.B. Ramos, J.C. Martins, M.J. Neves, F.P. Pires, Multicomponent solute transport in soil lysimeters irrigated with waters of different quality, Water Resour. Res., 42 (2006), doi: 10.1029/2005WR004802.
[9] T.B. Ramos, J. Šimůnek, M.C. Gonçalves, J.C. Martins, A. Prazeres, N.L. Castanheira, L.S. Pereira, Field evaluation of a multicomponent solute transport model in soils irrigated with saline waters, J. Hydrol., 407 (2011) 129–144.
[10] J. Šimůnek, M. Th. van Genuchten, M. Šejna, The HYDRUS Software Package for Simulating the Two- and Three-Dimensional Movement of Water, Heat, and Multiple Solutes in Variably-Saturated Media, Technical Manual, Version 1, PC Progress, Prague, Czech Republic, 2006.
[11] M.G. Schaap, F.J. Leij, M. Th. van Genuchten, Neural network analysis for hierarchical prediction of soil hydraulic properties, Soil Sci. Soc. Am. J., 62 (1998) 847–855.
[12] M. Th. van Genuchten, A closed-form equation for predicting the hydraulic conductivity of unsaturated soils, Soil Sci. Soc. Am. J., 44 (1980) 892–898.
[13] R.F. Carsel, R.S. Parrish, Developing joint probability distributions of soil water retention characteristics, Water Resour. Res., 24 (1988) 755–769.
[14] W.J. Rawls, D.L. Brakensiek, K.E. Saxtonn, Estimation of soil water properties, Trans. ASAE, 25 (1982) 1316–1320.
[15] J. Glass, J. Šimůnek, C. Stefan, Scaling factors in HYDRUS to simulate a reduction in hydraulic conductivity during infiltration from recharge wells and infiltration basins, Vadose Zone J., 19 (2020) e20027, doi: 10.1002/vzj2.20027.